

A High Energy Electron and Photon Detector Simulation System

Srikanta Sinha

3A, Sharda Royale Apt., 1 A Main, G M Palya, Bangalore-560 075, INDIA

email: srikanta_joy@yahoo.com

1 Abstract

A detailed Monte-Carlo code has been developed from basic principles that simulates almost all of the basic photon and charged particle interactions. The code is used to derive the response functions of a high energy photon detector to incident beams of photons of various energies. The detector response matrices(DRM)s are calculated using this code. Deconvolution of an artificially generated spectrum is presented.

Keywords: Simulation, Detector response matrix, spectral deconvolution

2 Introduction

The objective of the present endeavour is to develop a simple and user-friendly detector simulation code. An output pulse height spectrum is generated by the present code that may be compared directly with a measured pulse height spectrum which is the observable distribution.

The aim here is not to try to develop a simulation system as detailed and sophisticated as say, the EGSnrc or GEANT4 software systems but one that has all the basic physical processes incorporated within it and one which is, at the same time, sufficiently simple so that it may be used with ease to compare results of experiments where not very elaborate and complicated calibration systems are available- hence the calibration data also has certain inherent uncertainties and limitations due to effects (of say, surrounding materials etc.) that are neither well understood nor properly taken care of. In other words the present simulation code will be very useful in applications where extremely accurate results are not needed but a few percent accuracy will suffice.

The approach taken here is to develop the entire detector simulation code starting from the very basic principles, generate artificial photon input energy spectra, let these interact with the detector to give rise to output pulse height spectra. Using the detector calibration data, the pulse height spectra may be converted to equivalent output energy spectra. Since the DRMs are calculated using the same program, the output energy spectra can be deconvolved using these DRMs and the deconvolved spectra can be compared with the original input photon spectra. This procedure establishes, to a large extent, the validity and accuracy of the entire simulation code.

The simulation code is written in FORTRAN 77. The GNU compiler g77 is used to compile the code. It runs under Redhat Linux 9.0 operating system. A typical run to simulate a few thousand events for input photons say, 661 keV takes a few seconds in a PENTIUM IV system. This gives the energy deposition spectrum. In order to get the pulse height spectrum one has to use the photo-multiplier dynode multiplication simulation procedure. This takes rather long time, typically more than two hours for a few thousand events of 661 keV photons. The present code is nearly 3000 lines long

(excluding the data statements and the matrix inversion procedures). There are plans to rewrite the entire code in FORTRAN 90/95.

3 The Detector Geometry and Co-ordinate Systems

In the present simulations the detector geometry assumed is a cylindrical one. The center point of the detector is chosen to be the origin (O) of the global coordinate (right-handed rectangular Cartesian) system. The view axis of the detector is chosen to be the positive Z-axis of this co-ordinate system.

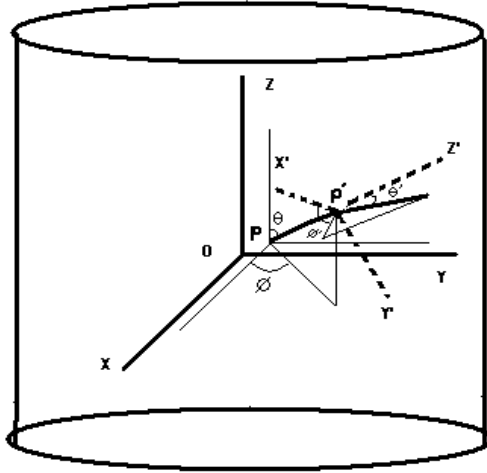


Figure 1: The global (OXYZ) and local (P'X'Y'Z') co-ordinate systems in the cylindrical geometry.

3.1 Co-ordinate Transformations:

Let a photon/particle start from a point P (x,y,z) and let its velocity (momentum) vector has a polar angle of θ and azimuth of ϕ with respect to the global co-ordinate system. If an interaction takes place at a geometrical distance $d_{int}(= d_{gm}/\rho)$ where d_{gm} is the distance in gcm^{-2} , ρ being the density of the medium, the co-ordinates of the interaction point P'(x',y',z') with respect to the global frame may be written as (Fig.1)

$$x' = x + d_{int} \sin\theta \cos\phi \quad (1)$$

$$y' = y + d_{int} \sin\theta \sin\phi \quad (2)$$

and

$$z' = z + d_{int} \cos\theta \quad (3)$$

In the event of an interaction, let a product particle/photon be emitted at a polar angle θ' and azimuth ϕ' where the Z'-axis of the local co-ordinate system is along the velocity

(momentum) vector of the product particle/photon. The values of θ' and ϕ' in the local co-ordinate system are transformed back to the global system (Θ , Φ) as follows:

$$\begin{pmatrix} \sin\Theta\cos\Phi \\ \sin\Theta\sin\Phi \\ \cos\Theta \end{pmatrix} = \begin{pmatrix} \cos\theta\cos\phi & -\sin\phi & \sin\theta\cos\phi \\ \cos\theta\sin\phi & \cos\phi & \sin\theta\sin\phi \\ -\sin\theta & 0 & \cos\theta \end{pmatrix} \begin{pmatrix} \sin\theta'\cos\phi' \\ \sin\theta'\sin\phi' \\ \cos\theta' \end{pmatrix} \quad (4)$$

Procedures have also been developed for rectangular geometry. Trial runs with these procedures gave encouraging results.

4 Cross Sections

Cross sections for all the different types of interactions of photons and charged particles are necessary to simulate these processes within the detector material. Since the composition of the detector material is unknown a priori, cross section tables for all elements should be available to the program. At present the atomic cross section tables for only the following elements are available, viz. Hydrogen, Carbon, Sodium, Argon, Iodine, Xenon and Cesium. Near the absorption edges the cross sections are calculated for many closely spaced energy values. The XCOM program developed by Berger and Hubbell [1] is used for this purpose. This program is used to calculate the photo-electric, coherent, incoherent and pair production cross-sections.

In the XCOM program, the coherent (Rayleigh) scattering cross sections are calculated using a combination of the Thompson formula and relativistic Hartree- Fock atomic form factors.

In XCOM, the photo-electric cross sections are obtained following the method of Scofield [2] upto 1.5 MeV of input photon energy. At higher energies a semi-empirical formula [3] and the asymptotic high energy limit calculated by Pratt [4] is used.

In XCOM, the incoherent (Compton) scattering cross sections are obtained using a combination of the Klein-Nishina formula and non-relativistic Hartree- Fock incoherent scattering functions.

For pair production, XCOM uses combinations of formulas from Bethe-Heitler theory [5] alongwith other theoretical models to take into account screening, Coulomb and radiative corrections. Please refer to ref.1 for the details of the XCOM program. Bremsstrahlung cross section is calculated separately.

The total cross section for electron bremsstrahlung is taken as

$$\sigma_{rad} = 4\sigma_o[\ln(183Z^{-1/3} + 1/18)] \quad (5)$$

where $\sigma_o = \alpha Z^2 r_e^2$, α is the fine structure constant, Z is the atomic no. of the material. r_e is the classical electron radius. Photon and charged particle interaction cross section tables are prepared for a wide range of energies, viz. 1 keV to 1000 MeV.

Given the cross sections for the elements, the cross section for a composite material (such as CsI) for any process may be calculated as

$$\sigma = \sum n_i \sigma_i \quad (6)$$

where n_i is the number of atoms per unit volume of the i th element constituting the material.

4.1 The Radiation Length

The radiation length X_0 is calculated as follows:

$$1/X_0 = 4\alpha N/AZ(Z+1)r_e^2 \ln(183Z^{-1/3}) \quad (7)$$

Here N is the Avogadro's number and A is the mass number of the element.

For a composite material the radiation length is given by the formula

$$1/X_0 = p_1/X_1 + p_2/X_2 \quad (8)$$

where p_1, p_2, \dots , are the fractional weights of the various components and X_1, X_2, \dots , are the corresponding radiation lengths.

5 Simulations of Different Processes

5.1 Photon Interactions

For photons four different types of interactions are considered. These are: (i) Coherent scattering, (ii) Photo-electric absorption, (iii) Incoherent scattering and (iv) Pair production. Atomic relaxations are considered in the cases of Photo-electric absorption and Compton scattering.

The geometrical distance of an interaction (d) from the point of incidence/previous interaction of the high energy photon is calculated from the equation

$$d = -\lambda \ln R \quad (9)$$

where R is a uniform random number between 0 and 1. All the uniform random numbers between 0 and 1 are generated using the fortran `RAND()` function. λ is the mean free path (reciprocal of the total photon interaction cross section of the detection medium at the given energy).

$$1/\lambda = \sigma_{coh.} + \sigma_{p.e.} + \sigma_{inc.} + \sigma_{pair} \quad (10)$$

where $\sigma_{coh.}$, $\sigma_{p.e.}$, $\sigma_{inc.}$ and σ_{pair} are respectively the coherent, photo-electric, incoherent and pair production cross sections. The value of the pair production cross section is, of course, equal to zero below a photon energy of 1.022 MeV. The type (K) of the interaction (one of the four types mentioned above) is determined using the relative (fractional) probability (cross section) for the specific process using a Russian Roulette, i.e.

$$p_k = \sigma_k / \Sigma \sigma_k \quad (11)$$

σ_k and p_k being respectively the cross section and the relative probability for the process K .

In the following we present the details of the algorithms used to simulate each of the above mentioned interactions.

5.2 Photo-electric Absorption:

In the photo-electric interaction with the atom, the incoming photon disappears and an electron is emitted whose energy equals the photon energy minus the binding energy of the electron in the relevant atomic shell.

$$E = E_p - \phi \quad (12)$$

where the symbols have their usual meanings. The atom then undergoes relaxation through either fluorescent photon emission or non-radiative transition (described later).

5.3 Incoherent (Compton) Scattering:

To simulate the incoherent scattering process first the atomic species is selected using a Russian Roulette (based on the relative incoherent scattering cross sections of the different constituent atoms of the detector material). Next, the relevant atomic shell is selected using the occupation numbers of the different atomic shells, Z_i/Z . The scattering angle (polar) θ of the photon in the local co-ordinates (the Z' axis of the local co-ordinate system points along the momentum vector of the interacting photon) is generated using the Klein-Nishina formula for the differential scattering cross section

$$d\sigma/d\Omega = Zr_e^2(1/1 + \alpha(1 - x))^2(1 + x^2/2)(1 + \alpha^2(1 - x)^2/(1 + x^2)[1 + \alpha(1 - x)]) \quad (13)$$

Here $x = \cos\theta$, θ being the polar angle of the scattered photon. $\alpha = 1/137$ is the fine structure constant and r_e is the classical electron radius. The von Neumann rejection technique is used for this purpose. Binding energy effects are taken into account by considering only those energy transfers to the electron that are larger than its binding energy. Doppler broadening effects are neglected.

The energy of the scattered photon $h\nu'$ is calculated using the formula

$$h\nu' = h\nu/[1 + (h\nu/m_o c^2)(1 - \cos\theta)] \quad (14)$$

ν being the frequency of the incident photon. h , m_o and c are respectively the Planck's constant, the electron rest mass and the velocity of light. The azimuth ϕ is uniformly generated between 0 and 2π .

The polar scattering angle θ_e (in the local system) of the recoil electron is calculated as

$$\theta_e = \tan^{-1}(1/(1 + \alpha)\tan(0.5\theta_p)) \quad (15)$$

where θ_p is the scattering angle of the photon and $\alpha = h\nu/m_o c^2$. The azimuth ϕ' of the recoil electron is equal to $(\pi - \phi_p)$ while its energy E_e is given by

$$E_e = E - E_p \quad (16)$$

5.4 Coherent Scattering:

The angular distribution $d\sigma_{coh}/d\Omega$ for coherent (Rayleigh) scattering is given approximately, by the distribution function $d\sigma_T/d\Omega$ for classical Thomson scattering by an electron,

$$d\sigma_T/d\Omega = r_e^2/2(1 + \cos^2\theta) \quad (17)$$

5.5 Electron-Positron Pair-production

The screening parameter γ is defined as

$$\gamma = 100(m_o c^2/E)[1/v(1 - v)]Z^{-1/3} \quad (18)$$

where

$$v = (E' + m_o c^2)/E \quad (19)$$

Here E is the energy of the photon that undergoes pair production into a positron having total energy E' and an electron having total energy $E - E'$. m_o is the electron rest mass, c the velocity of light and Z is the atomic number of the target nucleus. The differential cross section for pair production $\Phi_{pair}(E, E')$ depends on the value of the screening parameter. The theoretical expression for $\Phi_{pair(E, E')}$ is given by [6] as

$$\Phi_{pair}(E, E')dE' = 4\alpha N(Z^2/A)r_e^2(dE'/E)G(E, v) \quad (20)$$

For different ranges of the value of the screening parameter, the following expressions are used. No screening ($\gamma \gg 1$):

$$G(E, v) = [v^2 + (1 - v)^2 + (2/3)v(1 - v)][\ln(2E/m_0c^2)v(1 - v) - 1/2] \quad (21)$$

Complete screening ($\gamma = 0$):

$$G(E, V) = [v^2 + (1 - v)^2 + (2/3)v(1 - v)]\ln(183Z^{-1/3}) - (1/9)v(1 - v) \quad (22)$$

Intermediate cases ($0 < \gamma < 2$):

$$G(E, v) = [v^2 + (1 - v)^2][f_1(\gamma)/4 - (1/3)\ln Z] \quad (23)$$

($2 < \gamma < 15$):

$$G(E, v) = [v^2 + (1 - v)^2 + (2/3)v(1 - v)][\ln(2E/m_0c^2)v(1 - v) - 1/2 - c(\gamma)] \quad (24)$$

The functions $f_1(\gamma)$, $f_2(\gamma)$, and $c(\gamma)$ are the same that enter in the expressions for the radiation probabilities mentioned in subsection 7.1. For very small energy, k very near to $2m_0c^2$, Hough's approximate formula

$$\Phi(E_+)dE_+ = 8/3\Phi_0(k - 2m_0c^2/k)^3 z dE_+ \quad (25)$$

is used, where

$$z = 2\sqrt{x}(1 - x) \quad (26)$$

and x is given by

$$x = E_+ - m_0c^2/k - 2m_0c^2 \quad (27)$$

The angle of the positron (electron) with respect to the momentum vector of the high energy photon (Z' axis of the local system) is given by

$$\theta = m_0c^2/E_{\pm} \quad (28)$$

5.6 Muon Pair Production:

The formulae given in the previous subsection may be used to simulate $\mu^+ - \mu^-$ pairs although the threshold for this process is equal to 206 times the threshold for the corresponding process for $e^+ - e^-$ pair, i.e. 210.532 MeV.

6 Atomic Relaxations:

In the case of photo-electric absorption and also in the case of incoherent scattering, a vacancy is created in the electronic shell with which the photon interacts. This vacancy is filled by electrons from higher energy shells and the excitation energy is released in the form of either (i) one or more fluorescent photons, (ii) an Auger electron, or (iii) a Coster-Kronig electron. The relative probabilities for these three types of relaxation processes are different for different electronic shells. In the present work the Coster-Kronig process is neglected.

6.1 Fluorescence

The energy of the fluorescence photon is equal to the difference in the binding energies of the initial and final states of the atom. The fluorescent X-ray photon is emitted isotropically. Its polar angle (θ) and azimuth (ϕ) in the local system are calculated as follows:

$$\theta = \cos^{-1}(2R_1 - 1) \quad (29)$$

and

$$\phi = 2\pi R_2 \quad (30)$$

R_1 and R_2 being two different random numbers that are distributed uniformly between 0 and 1. The values of θ and ϕ are transformed back to the global co-ordinate system using eqns.(1) and (2).

The fluorescent photon may, either (i) escape the detection medium (the location of its interaction being outside the boundary of the detector and in that case its energy is treated as lost resulting in an energy deposit that is equal to the input photon energy minus the fluorescent photon energy. This kind of events give rise to the characteristic X-ray escape peak), or, (ii) it may interact photo-electrically with a higher shell in which case either its total energy or a part of its energy (in the case of escape of a higher shell fluorescent photon) is deposited.

6.2 Auger Electron Emission

The Auger electron emission (non-radiative electron emission) is considered only for the K and L shells. The energy(ies) of the Auger electron(s) is completely absorbed within the detection medium and contribute to the energy deposited.

7 Charged Particle Interactions:

For electrons, bremsstrahlung and for positrons, bremsstrahlung and pair annihilation processes are considered. For electrons and positrons multiple Coulomb scattering is considered in an approximate manner.

7.1 Bremsstrahlung

The Bremsstrahlung process is essentially similar to the pair production phenomenon.

The differential cross section (probability) for the radiation process, $\Phi_{rad}(E, E')$ depends on the value of the screening parameter which is defined as

$$\gamma = 100(m_0c^2/U)[v/(1-v)]Z^{-1/3} \quad (31)$$

Here,

$$U = E + m_0c^2 \quad (32)$$

and

$$v = E'/U \quad (33)$$

The expression for $\Phi_{rad}(E, E')$ is given by ref.6 as

$$\Phi_{rad}(E, E')dE' = 4\alpha(N/A)Z^2r_e^2(dE'/E')F(U, v) \quad (34)$$

For different ranges of the value of γ , the differential cross section is given by the following formulas: No screening ($\gamma \gg 1$):

$$F(U, v) = [1 + (1-v)^2 - (2/3)(1-v)][\ln(2U/m_0c^2)(1-v)/v - 1/2] \quad (35)$$

Complete screening ($\gamma = 0$):

$$F(U, v) = [1 + (1 - v)^2 - (2/3)(1 - v)]\ln(183Z^{-1/3}) + 1/9(1 - v) \quad (36)$$

Intermediate cases, ($0 < \gamma < 2$):

$$F(U, v) = [1 + (1 - v)^2][f_1(\gamma)/4 - (1/3)\ln Z] - (2/3)(1 - v)[f_2(\gamma)/4 - (1/3)\ln Z] \quad (37)$$

($2 < \gamma < 15$):

$$F(U, v) = [1 + (1 - v)^2 - (2/3)(1 - v)][\ln(2U/m_0c^2)(1 - v)/v - 1/2 - c(\gamma)^{1/2}] \quad (38)$$

The average angle of the emitted photon with respect to the momentum vector of the high energy electron (Z' axis of the local system) is given by

$$\theta_0 = m_0c^2/E_0 \quad (39)$$

7.2 e^+e^- Annihilation

Only electron-positron pair annihilation at rest is presently considered. The energy of each annihilation photon is equal to 0.511 MeV. The direction of the second photon is taken to be exactly opposite to the direction of the first photon which is sampled from a distribution that is isotropically distributed.

7.3 Knock-On (δ ray) production

High energy electrons often produce electrons of energies that are comparable to the energies of the primary electrons. This process is simulated using the formula [7]

$$P(E)dE = WdE/E^2 \quad (40)$$

where $P(E)dE$ is the probability of an electron receiving the energy E . W is a constant that depends on Z , A ; the atomic number and the mass number of the medium in addition to the velocity β of the primary electron.

7.4 Multiple Coulomb Scattering

The well-known Moliere theory of Coulomb scattering is used in order to take into account the scattering of light charged particles (electrons and positrons) in the Coulomb fields of both atomic nuclei and atomic electrons.

For this the energy domain is divided into two intervals. The first interval includes charged particles whose energies lie between 1 keV and 1 MeV. The second interval includes the energy region between 1 MeV and 1 GeV. These two energy intervals are again subdivided each into 30 logarithmic energy bins (following the treatment used by Vatcha [8]). For charged particles having energies above 1 GeV, only a gaussian having a width equal to $(E_s/E\beta)\sqrt{t}$, (where E is the energy of the particle, $\beta = v/c$, v being its velocity and $t = x/X_0$ is the thickness of the slab of material in terms of its radiation length) is considered. The constant $E_s = 21$ MeV.

Bethe [9] has expressed Moliere's theory of multiple Coulomb scattering in a form which is easy to simulate. Using the first two terms of his equation () together with a correction for solid angle the frequency function for scattered angle is

$$f(\Theta)d\Theta = (\sin\Theta/\Theta)^{1/2}[f^{(0)}(\phi) + 1/Bf^{(1)}(\phi)]\phi d\phi \quad (41)$$

Here ϕ is the reduced angle of Θ which is defined as

$$\phi = \Theta/\chi_c B^{1/2} \quad (42)$$

where

$$\chi_c^2 = 0.157Z(Z+1)t/A(pv)^2 \quad (43)$$

where pv is in MeV, t is in grams per square centimeter, and A is the atomic weight of the material. The parameter B is defined by the transcendental equation

$$B - \ln B = B' \quad (44)$$

where

$$B' = 2\ln(\chi_c/\chi_a) + 1 - 2C \quad (45)$$

where $C = 0.577\dots$ is Euler's constant and χ_a is an angle which depends on the screening of the atomic field. It is defined as

$$\chi_a^2 = (\lambda/5.561a_0Z^{-1/3})^2(1.13 + 3.76\alpha^2) \quad (46)$$

with

$$\alpha = 2\pi zZ^2/hv \quad (47)$$

The functions $f^{(0)}(\phi)$ and $f^{(1)}(\phi)$ are defined as

$$f^{(0)}(\phi) = 2e^{-\phi^2} \quad (48)$$

and

$$f^{(1)}(\phi) = f^{(0)}(\phi)(\phi^2 - 1)(Ei(\phi^2) - \ln(\phi^2) - 2(1 - f^{(0)}(\phi))) \quad (49)$$

where $Ei(x)$ is defined as follows:

$$Ei(x) = - \int_{-x}^{\inf} e^{-t}/tdt = \int_{-\inf}^x e^t/tdt \quad (50)$$

For a given electron energy a slab thickness (proportional to the energy of the electron) of the material is chosen. The percentage probability of scattering is selected using a uniform random number between 0 and 1. The angle of scattering is selected from the table using reverse interpolation [10].

7.5 Ionisation Loss and Particle Ranges

For the ionisation loss the expression given by Bethe and Bloch in ref.7 is used.

$$dE/dx = (1/\rho)dE/dX \quad (51)$$

Here $x = X\rho$ is in $gmscm^{-2}$ while X is in cms.

$$dE/dX = -K(Z/A)(\rho/\beta^2)[\ln 2m_o c^2 \beta^2 E_M/I^2(1 - \beta^2) - 2\beta^2] \quad (52)$$

where

$$K = 2\pi N z^2 e^4 / m_o c^2 \quad (53)$$

Here N is the Avogadro number, m_o and e are mass of the electron and its charge, Z , A and ρ are the atomic number and the mass number and the density of the medium, respectively, and I is its effective ionization potential; z is the charge and β the velocity (in units of c , the speed of light) of the incident particle.

E_M represents the maximum possible energy transfer in an interaction and is given by

$$E_M = 2m_0c^2\beta^2/(1 - \beta^2) \quad (54)$$

For energies of electrons (δ rays) an approximate formula for the practical range, in gcm^{-2} is used (ref.7)

$$R_p = 0.71E^{1.72} \quad (55)$$

where the energy of the electron (E) is expressed in MeV.

7.6 Emission of Scintillation Photons

The number of scintillation photons (integrated over the spectral band) produced in the scintillator is obtained simply by dividing the energy deposited by a constant that gives the average energy required to produce a scintillation photon. The value of this constant is 0.02564 eV for CsI [11]. Since the number of scintillation photons is always an integer, 0.5 is added to the calculated value and the result is truncated.

7.7 Emission of Cerenkov Photons

In case the charged particles produced in any of the interactions happen to traverse regions that consist of transparent media (such as air, water, plastics etc.) and the velocity of the particles exceed the velocity of light in those media, Cerenkov photons are emitted.

The angle of emission θ_C of the Cerenkov photons is given by the equation

$$\cos\theta_C = 1/n\beta \quad (56)$$

where β is equal to v/c , v being the velocity of the particle, while n represents the refractive index of the local medium. The number of Cerenkov photons dN emitted in the track length element dl in the wavelength interval $\Delta\lambda$ is given by the equation

$$dN = 2\pi\alpha dl(1 - 1/n^2\beta^2)\Delta\lambda \quad (57)$$

The spectral distribution of Cerenkov photons is sampled using the probability distribution

$$P(\lambda)d\lambda = (1.0/\lambda^2)d\lambda \quad (58)$$

7.8 Charge Multiplication at the Photomultiplier:

The scintillation photons incident on the photo-cathode (N_i) of the photo multiplier (PMT) are converted into a photo-current (number of photo-electrons, N_e)

$$N_e = \langle \eta \rangle N_i \quad (59)$$

where $\langle \eta \rangle$, the average spectral efficiency of the photo-cathode is taken to be equal to 0.2. $\langle \eta \rangle$ depends on the spectral response of the particular photocathode type. Strictly speaking,

$$N_e = \int N_i(\lambda)\eta(\lambda)/\int \eta(\lambda) \quad (60)$$

where $N_i(\lambda)$ is the number of scintillation photons having wavelength λ and $\eta(\lambda)$ is the corresponding spectral efficiency.

The photo-electrons are multiplied by the successive dynodes (8 to 10 in number) through secondary emission process.

The energy resolution of the detector is determined largely by the statistical fluctuations in the minimum number of particles (electrons) in the dynode chain, i.e. the number of photo-electrons. The charge multiplication at the dynodes is simulated in the following manner.

Using the knowledge of the total PMT high voltage and its distribution between different dynodes (usually all the dynode voltages are equal except the first one), from the PMT data book the average secondary electron multiplication factors are obtained. Since the electron multiplication is a Poisson process, in each successive stage this multiplication is simulated using a previously calculated table of Poisson probabilities for obtaining an integral number of secondary electrons for a given average value.

7.9 Folding the Radial Response in the case of scintillation detectors

It has been observed that in scintillation detectors, the photomultiplier tube light collection efficiency reduces to 85% near the edge of the crystal for a given energy deposition, as compared to the same energy deposited at the center of the crystal. This radial radial response function (a quadratic fit to light collection vs. radial distance of the point of energy deposition) is used to obtain the amount of light incident at the photo-cathode of the PMT.

7.10 Charge Integration and Pulse Height Spectrum

The charge output at the anode of the PMT is integrated into a charge sensitive pre-amplifier (CSPA) having a charge gain equal to 0.025×10^{12} Volts/Coulomb, thus producing a voltage pulse as output. This is amplified using a linear amplifier of gain equal to 5.

7.11 Calibrating the Detector

The detector is calibrated as follows: The response functions (the pulse height spectra) are simulated for two monoenergetic incident photons (say, 100 keV and 600 keV) using a large (say, 10 000) number of incident photons. The positions of the photo-peaks (full energy peaks) are determined accurately using very fine binnings. A straight line fit is obtained with the pulse height as a function of the input photon energy

$$h = mE + b \tag{61}$$

h being the pulse height in volts and E being the photon energy in keV. The calculated values of m and b are used to convert output pulse heights into corresponding energy values to form the output energy spectra.

8 Generation of Artificial Photon Input Spectrum and Spectral Deconvolution:

In order to check the correctness of the calculated DRMs it is necessary to generate artificial photon energy spectra, let them interact with the detector and obtain output pulse height spectra. These pulse height spectra should then be deconvolved back into photon energy spectra using the calculated DRMs. These deconvolved photon spectra should be compared with the original photon spectra using say, χ^2 tests. This procedure would then establish the correctness of the entire detector simulation code.

8.0.1 Power-Law Photon Energy Spectrum

A power-law (differential) photon energy spectrum having the form $AE^{-\gamma}$ where A is the normalisation constant, E the energy of the photon and γ is the spectral (differential) index, is generated using the inverse transform method as follows:

$$E = (KR + k_1)^{1/(1-\gamma)} \quad (62)$$

where $K = E_2^{(1-\gamma)} - k_1$ and $k_1 = E_1^{(1-\gamma)}$. E_1 and E_2 are respectively the minimum and maximum limits of the spectral energy band. R is a random number uniformly distributed between 0 and 1.

An input spectrum of photons (power law) is simulated. The corresponding output pulse height spectrum is converted to an equivalent energy spectrum (using the artificial calibration data). Let \mathbf{P} be the vector that represents the output pulse height spectrum (rebinned) and \mathbf{R} the detector response matrix. If the true input photon energy spectrum is denoted by the vector \mathbf{S} , then

$$\mathbf{P}_i = \sum \mathbf{R}_{ij} \mathbf{S}_j \quad (63)$$

where \mathbf{P}_i is the detected counts in the i th energy channel, \mathbf{S}_j the number of input photons in the j th energy channel and \mathbf{R}_{ij} is the ij th element of the DRM. The true incident photon spectrum \mathbf{S} is obtained by the matrix inversion procedure.

$$\mathbf{S} = \mathbf{R}^{-1} \mathbf{P} \quad (64)$$

where \mathbf{R}^{-1} is the inverse of the detector response matrix (historically, the first such detector response matrix was calculated by J. H. Hubbell [12]).

8.1 Simulation of Gamma Ray Burst (GRB) Spectrum

The energy spectrum of Gamma Ray Burst sources are best described by the Band [13],[14] spectrum. A typical Band spectrum is given as

$$N(E) = A(E/100)^\alpha \exp(-E/E_0) \quad (65)$$

for

$$E \leq (\alpha - \beta)E_0 \quad (66)$$

and

$$N(E) = A(\alpha - \beta)(E_0/100)^{\alpha-\beta} (E/100)^\beta \quad (67)$$

for

$$E > (\alpha - \beta)E_0$$

9 Gamma Ray Applications

In the case of gamma ray studies, the detector (e.g. a CsI scintillator) is usually shielded using a plastic scintillator that is used as a veto counter to remove the charged particle background. Usually there is a thin window (say, of Aluminium) in front of the scintillator. In addition a metal casing is used to cover the detector. Gamma rays interact in all of these materials and produce either coherently scattered gamma ray photons having energies equal to that of the primary, or, they may produce incoherently scattered photons of lower energies or they may also produce annihilation gamma rays. These secondary photons have finite chances of entering the actual detection volume (in this case the CsI crystal). Sometimes they may be scattered from another material and enter

the scintillator though the probabilities of such tertiary and higher order scatterings are small.

These effects are taken care of in the following manner. Nested volumes of materials are considered where the actual detection volume (in this case CsI) is designated as the volume of zeroth order. The next set of volumes (composition will in general be very different) that enclose the zeroth volume is called the volumes of first order and so on. When a primary gamma ray is incident on any of the volumes, its history is traced until either it misses or hits the zeroth volume. If it misses the zeroth volume it is rejected while in the other case it is considered as a valid incident photon of degraded energy. Development of this procedure is yet to be completed.

10 Results

In the following the results of simulations for a Cesium Iodide scintillation detector (3 inch diameter and 0.5 inch thickness) are presented.

10.1 Detector Efficiency

The efficiency of a Cesium Iodide scintillation detector has been estimated from the simulations. These estimated values of the detector efficiency are plotted in Fig.2.

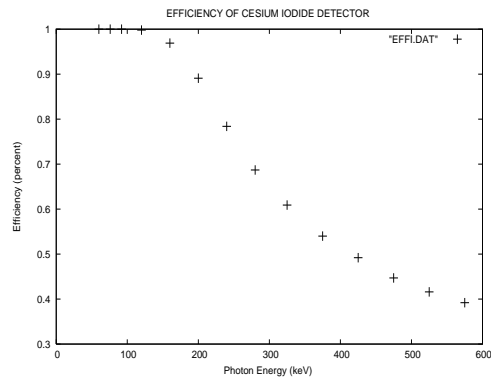


Figure 2: The efficiency of the CsI detector (3 inch diameter and 0.5 inch thickness) is plotted as a function of energy.

10.2 Energy Resolution of the Detector

From the simulations the energy resolutions of a Cesium Iodide scintillation detector has been derived at various energy values. The energy resolution is obtained by dividing the full width at half maximum (FWHM) of the photo-peak (full energy peak) by the energy of the photo peak. In Fig.3 the estimated energy resolutions are plotted against the energy of the incident high energy photon.

10.3 Sample Response Functions

In Fig.4 a sample response function is shown. The energy of the incident photons are each equal to 70 keV. In Fig.4 the peak near 20 keV is due to the escape of the characteristic X-ray fluorescence photons. For Cesium and Iodine, the energies of these photons are respectively 35.98 and 33.17 keV. In Fig.5 the response function of the same detector for

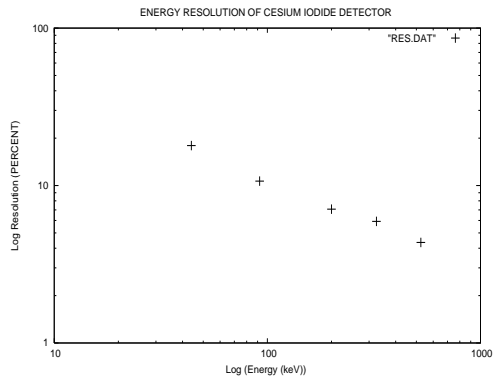


Figure 3: The energy resolution of the CsI detector is plotted as a function of energy. The $E^{-1/2}$ dependence of the energy resolution is clearly evident in the figure.

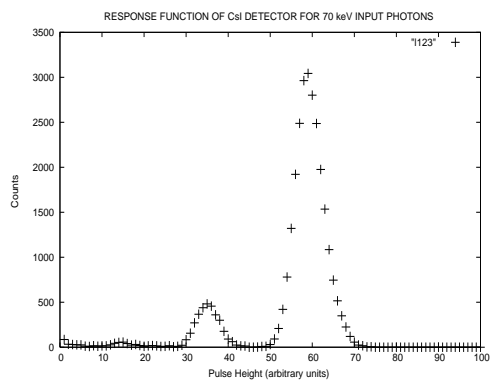


Figure 4: Simulated response function of the CsI scintillator to an input beam of 70 keV photons. The K X-ray escape peak is clearly seen.

525 keV input photons are shown.

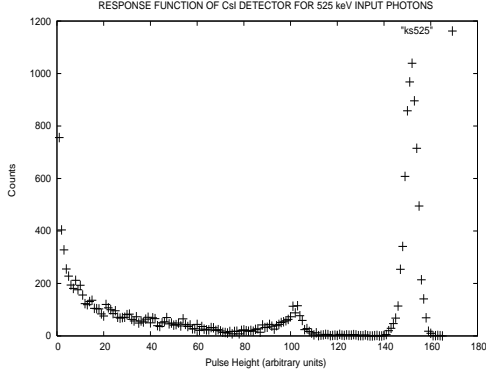


Figure 5: Simulated response function of the CsI scintillator to an input beam of 525 keV photons. The Compton edge and the Compton continuum are clearly visible.

10.4 Response Matrix and Spectral Deconvolution

The response functions of the CsI detector are calculated for the following 16 different energy values, viz. 28, 44, 60, 76, 92, 120, 160, 200, 240, 280, 325, 375, 425, 475, 525 and 575 keVs. These response functions are binned into the following energy intervals, viz. 12-30, 30-49, 49-68, 68-87, 87-106, 106-152, 152-199, 199-246, 246-293, 293-340, 340-398, 398-457, 457-516, 516-574 and 574-633 keV respectively. Thus, the response matrix (DRM) of the CsI detector is obtained.

A power-law (differential index equal to -1.38) photon spectrum is generated using the algorithm described in section 7.0.1. A total of 9 936 photons having their energies between 20 keV and 600 keV are generated. In addition, 70 photons having energy equal to 511 keV each are generated. These photons are made incident on the CsI scintillator at an angle of 1 degree relative to the view axis. These photons interact within the scintillation crystal and give the output spectrum depicted in fig.6. This output spectrum is obtained by binning the output energy spectrum using the energy intervals described in the previous paragraph.

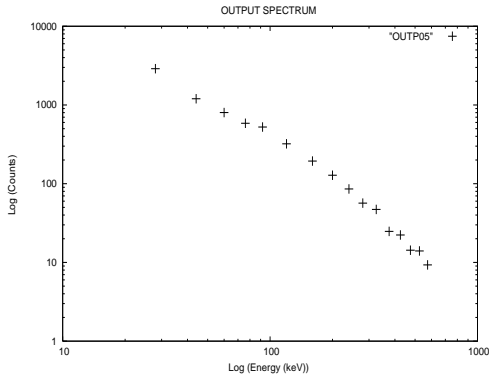


Figure 6: Simulated output spectrum from the detector for an input power law photon spectrum (differential index equal to -1.38). At higher energies the counts decrease due to the gradually decreasing efficiency of photon detection.

The inverse of the DRM is calculated using well established procedures [15]. The result of deconvolution of the output energy spectrum of fig.6 with this inverse of the DRM is shown in the following figure.

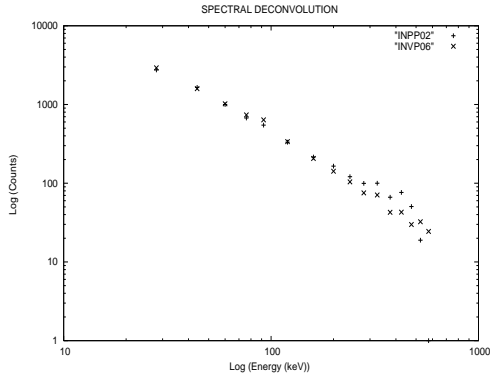


Figure 7: The deconvolved energy spectrum (crosses) is compared with the input photon spectrum (plus signs). The two spectra agree quite well at low and medium energies but seem not to match very well at the high energy end.

11 Results of Simulations of Other Interaction Processes

Pair production at high energies is simulated using the formulae given in section 4.5. The results are shown in the figure below. In Fig.8 the fractional energy (v) of the positron is plotted along the abscissa and the quantity $E\phi_{pair}(E, E')$ is plotted along the ordinate. Here $\phi_{pair}(E, E') = X_0\Phi_{pair}(E, E')$ is the differential pair production probability per radiation length. $\Phi_{pair}(E, E')$ is the differential pair production probability of production of a positron having energy E' by an incident photon having energy E in $1gcm^{-2}$ thickness of the material.

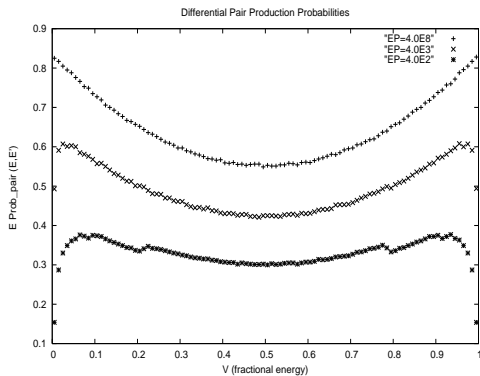


Figure 8: Simulated differential pair production probabilities at high energies. The values (inset) give the energies of the input photons in terms of the electron mass.

The pair production at low energies are simulated using the Hough's formulae given in section 4.5. The results of one such simulation is shown in the following figure.

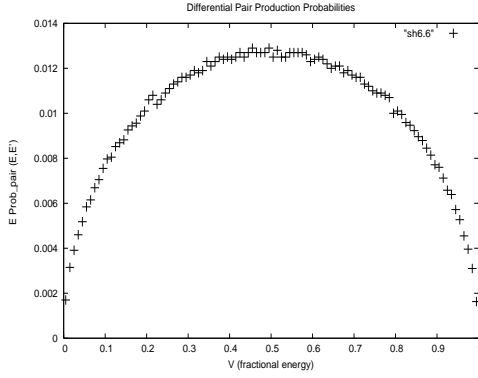


Figure 9: Simulated differential pair production probabilities at low energies. The value (inset) give the energy of the input photons in terms of the electron rest mass.

The electron/positron bremsstrahlung processes at high energies are simulated using the formulae given in section 6.1. The results of these simulations are given in fig.10. Here again the fractional energy (v) of the emitted photon is plotted along the abscissa and the quantity $E' \phi_{rad}(E, E')$, where $\phi_{rad}(E, E') = X_0 \Phi_{rad}(E, E')$, is the differential radiation probability per radiation length. $\Phi_{pair}(E, E')$ is the differential radiation probability of production of a photon having energy E' by an incident electron having energy E in $1gcm^{-2}$ thickness of the material.

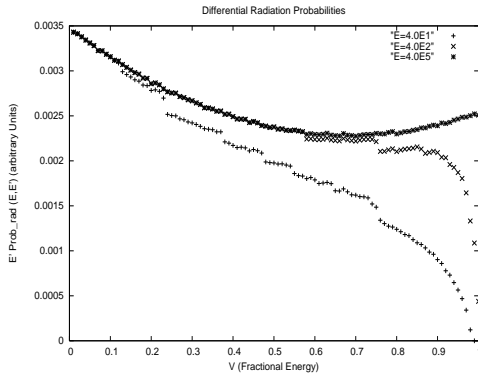


Figure 10: Simulated differential radiation probabilities at high energies. The values (inset) give the energies of the input electrons in terms of the electron rest mass.

Knock-on (delta ray) productions by a 10 MeV electron are simulated using the procedure described in section 6.3. The results are shown in fig.11.

Cerenkov photon emission by high energy electrons/positrons are simulated using the formulae given in section.6.7. The simulated wavelength spectrum of Cerenkov photons in the wavelength band of $300nm$ to $650nm$ is shown in the following figure.

12 Simulations of Photon Energy Spectra

Different sources emit different types of high energy photon spectra. It is necessary, therefore, to be able to simulate different types of photon energy spectra. In the following

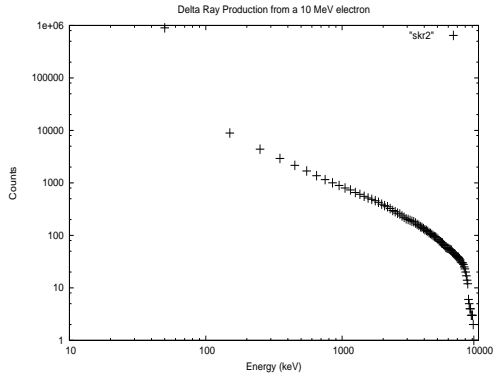


Figure 11: Simulated probability distribution for the production of delta rays (knock-on electrons) produced by an incident electron of energy 10 MeV.

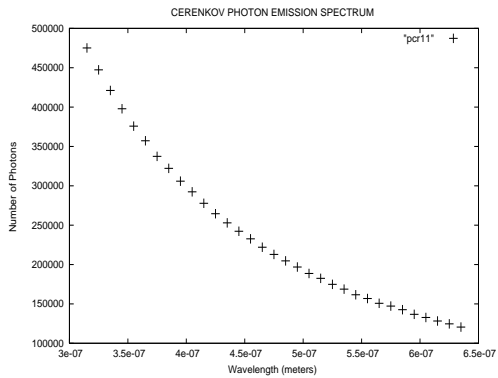


Figure 12: Simulated wavelength spectrum of cerenkov photons emitted by an electron/positron within the wavelength range of 300nm to 650nm.

two different types of spectra, viz. (a) a power-law energy spectrum (large number of photons- the total being equal to 9 million) and (b) a smoothly-broken power-law (Band Spectrum) spectrum are shown.

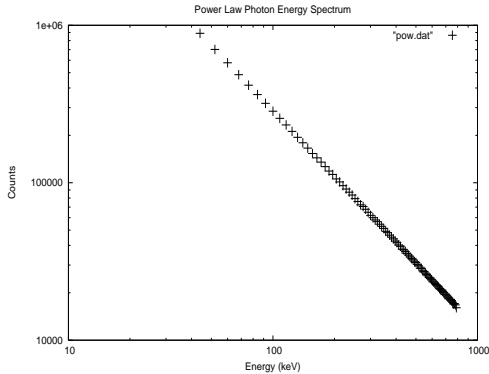


Figure 13: Simulated power-law energy spectrum of photons having a differential energy index of -1.38 .

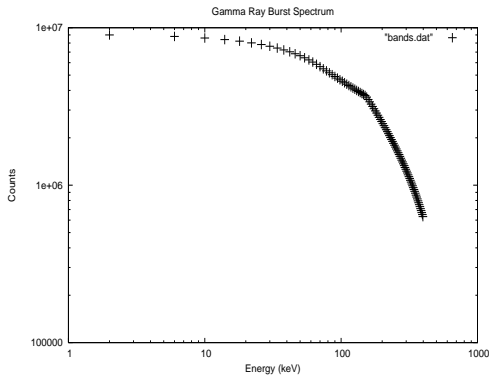


Figure 14: Simulated energy spectrum (Band spectrum) of a hypothetical gamma ray burst. The parameter values are: (i) $A = 1.0E4$, (ii) $\alpha = -1.0$, (iii) $\beta = -2.0$ and (iv) $E_0 = 150.0keV$.

13 Discussion

It is possible to incorporate any detector geometry (say, rectangular geometry) in the present simulation code and calculate the response of that detector. Also, the response functions of other types of detectors, for example, gas (Argon or Xenon) filled multi-wire proportional chambers (MWPCs) such as those used in X-ray astronomy experiments may be obtained.

In the present simulations the differential cross sections used for the coherent scattering and the incoherent scattering processes are respectively the classical Thomson cross section and the Klein-Nishina formula. Strictly speaking, in the case of coherent scattering the square of the atomic form factor $F(q, Z)$ should be multiplied with the Thomson cross section while in the case of incoherent scattering the incoherent scattering function

$S(x, Z)$ should be multiplied with the Klein-Nishina differential cross section. These changes will be introduced in a later version of the code.

All the different modes of atomic relaxations are yet to be incorporated in the present code. Pair annihilation in flight and triplet production are also to be introduced.

There are some small irregularities and discontinuities in the plots of the differential probabilities for pair production and bremsstrahlung (fig.5 and fig.7). Presumably these have resulted due to the fact that somewhat coarse interpolations of the three screening functions ($f_1(\gamma)$, $f_2(\gamma)$, and $c(\gamma)$) have been used in the present simulations.

There is minor disagreement of the deconvolved spectrum with the input photon spectrum (Fig.5) at the high energy end. This is due to the fact that the number of events in this energy range are small and the response functions at the higher energies are poorly determined (due to the insufficiency of the number of events generated to calculate the response functions).

14 Conclusions

A high energy photon detector simulation code developed from the first principles has been described. The results obtained using this code are quite encouraging. This code gives an output pulse height spectrum, instead of an energy loss spectrum. This simulation code is being developed further to incorporate all the possible interaction types of photons and particles. It should be possible to extend this code to simulate extensive air showers (EAS) in the atmosphere produced by very high energy (VHE) and ultra high energy (UHE) gamma rays and electrons and also to study the cerenkov radiation produced in these cascades.

15 Acknowledgements

I would like to express my deep sense of gratitude to all my revered teachers.

This research article is dedicated to the memory of late Prof. John H. Hubbell. I am greatly indebted to him and his collaborators at NIST for kindly supplying me the XCOM program. Prof. Hubbell had also given me a lot of relevant literature on photon cross sections as well as other material that were very helpful to my understanding. It is my bad luck that I could not finish this work before he passed away.

I thank Prof. Kevin Hurley and Prof. Fabio Sauli for their kind suggestions to improve the manuscript. Thanks are also due to Dr. Varsha Chitnis for her kind help. I thank my family for their patience and support.

References

- [1] M.J. Berger and J.H. Hubbell., XCOM: Photon Cross Sections on A Personal Computer, NBSIR 87-3597
- [2] J. H. Scofield., Theoretical Photoionization Cross Sections from 1 to 1500 keV, Lawrence Livermore National Laboratory Rep. UCRL-51326 (1973).
- [3] J. H. Hubbell., Photon Cross Sections, Attenuation Coefficients and Energy Absorption Coefficients from 10 keV to 100 GeV, Natl. Stand. Ref. Data Ser. 29 (1969).
- [4] R. H. Pratt., Atomic Photoelectric Effect at High Energies, Phys. Rev. 117, 1017-1028 (1960).

- [5] W. Heitler., The Quantum Theory of Radiation, 3rd ed., Oxford: Clarendon Press, 1953.
- [6] B. Rossi., High Energy Particles (Englewood Cliffs, NJ: Prentice-Hall).
- [7] F. Sauli, Lectures given in the Academic Training Programme of CERN (1975-1976), CERN 77-09.
- [8] R. H. Vatcha, Ph. D Thesis, University of Bombay (1972), Unpublished.
- [9] H. Bethe and J. Ashkin, Passage of radiation through matter, in E. Segre (ed.), Experimental Nuclear Physics, Vol.1, Part 2, New York: Wiley, 1959.
- [10] H. Bichsel, Nuclear Instruments and Methods in Physics Research B52 (1990) 136-139.
- [11] G. F. Knoll, Radiation Detection and Measurement, 2nd Ed., John Wiley & Sons, 1989.
- [12] J. H. Hubbell, The Review of Scientific Instruments, Vol. 29, No.1, 65-68, 1958.
- [13] D. Band et al, Ap. J, (1993), in press
- [14] B. E. Schafer et al Ap. J, 404 (1993), p.673
- [15] W. H. Press et al., Numerical Recipes (The Art of Scientific Computing), 2nd ed., Cambridge University Press, 1992.